

BUNCH COMPRESSION OF FLAT BEAMS

A. Halavanau^{1,2}, P. Piot^{1,2}, D. Edstrom Jr.¹, A. Romanov¹,
 D. Crawford¹, J. Ruan¹, D. Mihalcea¹, V. Shiltsev¹, S. Nagaitsev¹

¹ Fermi National Accelerator Laboratory, Batavia IL 60510, USA

² Department of Physics and Northern Illinois Center for Accelerator &
 Detector Development, Northern Illinois University DeKalb, IL 60115, USA

Abstract

Flat beams can be produced via a linear manipulation of canonical-angular-momentum (CAM) dominated beams using a set of skew-quadrupole magnets. Recently, such beams were produced at Fermilab Accelerator Science and Technology (FAST) facility ¹. In this paper we report the results of flat beam compression study in a magnetic chicane at an energy $E \sim 32$ MeV. Additionally, we investigate the effect of energy chirp in the round-to-flat beam transform. The experimental results are compared with numerical simulations.

INTRODUCTION

Flat beams are generated from canonical angular momentum dominated (CAM) beams via round-to-flat beam (RTFB) transformation [1]. Transverse and longitudinal beam dynamics of a flat beam in the FAST [2] chicane was numerically investigated in a great detail in [3]. In brief, a transverse emittance growth is expected during the flat beam compression in the chicane due to space-charge and coherent synchrotron radiation (CSR) effects in chicane doglegs. It was found that the emittance growth occurs mostly when the bunch length is the shortest, and additionally horizontal emittance growth was much larger than vertical [4]. The final emittance degradation associated to the induced energy spread over one dipole magnet in the bending plane is given by [5, 6]:

$$\epsilon_{x,f} \approx \sqrt{\epsilon_{x,i}^2 + \epsilon_{x,i} \beta_{x,f} \langle \Delta x'^2 \rangle}, \quad (1)$$

where $\epsilon_{x,f}$ and $\epsilon_{x,i}$ are respectively the final and initial geometric emittance, $\beta_{x,f}$ is the betatron function at the end of the bunch compressor and $\Delta x' \approx \theta \delta E / (2E)$. In the latter expression δ corresponds to the energy spread induced by the CSR effects, $\theta = 18$ degrees for FAST bunch compressor and E is the total energy of the electron beam. When the value of $\epsilon_{x,i}$ is large, the resulting emittance is mostly unaffected by the CSR induced angular spread. Thus, in case of a horizontal flat beam, since the emittance in the bending plane is $\epsilon_x \gg \epsilon_y$, therefore making the beam not susceptible to the emittance growth in that plane during compression. This fact also implies that the total ϵ_{4D} will be less degraded after the bunch compressor, making the ap-

plication of flat beams advantageous for the beam transport of short bunches in bending systems.

FLAT BEAM GENERATION AT FAST

CAM and flat beams were generated at FAST during Run-2017. We refer the reader to Ref. [7] for the detailed description of this experiment. At first, the settings of the RTFB adapter were calculated and optimized numerically [8]. The resulting comparison between experiment and simulations is presented in Fig. 2. One can see a good agreement between the numerically optimized solutions and the measured real beam distributions. The generated flat beam was propagated downstream of the RTFB adapter to ensure full transmission to the low energy adsorber. After the flat beam generation, the initial emittance measurement was performed with a quadrupole scan technique.

The beam transverse distribution was registered at the X121 location as a function of quadrupole Q120 current. FAST beamline was implemented into ELEGANT tracking code and the function SDDSEMITMEAS was invoked to fit the beam distribution emittances to the experimental data [9]. The initially recorded emittance values were not quite in agreement with the prediction given by [10–12], therefore we performed beam-based optimization of the round-to-flat beam transformation.

In order to optimize the mapping of the eigenemittances onto resulting flat beam emittances, we developed a beam-based optimization tool using the PYACL framework [13]. In the optimization procedure, skew quadrupoles Q106, Q107 and Q111 were used as free variables, while all the quadrupole magnets downstream of the Q111 were turned off. We set the ratio between beam transverse sizes at two locations (d_1, d_2) (corresponding to the screen X111/X121 positions; see Fig. 1) as a target function as:

$$\rho = \sqrt{\left(\frac{\sigma_{x,y}}{\sigma_{y,x}}\right)_{d_1}^2 + \left(\frac{\sigma_{x,y}}{\sigma_{y,x}}\right)_{d_2}^2} \\ = \sqrt{\left(\frac{\beta_{x,y} \epsilon_{x,y}}{\beta_{y,x} \epsilon_{y,x}}\right)_{d_1}^2 + \left(\frac{\beta_{x,y} \epsilon_{x,y}}{\beta_{y,x} \epsilon_{y,x}}\right)_{d_2}^2}.$$

In the latter equation, maximizing σ_x/σ_y means horizontal flat beam optimization and σ_y/σ_x corresponds to the case of vertical flat beam optimization. In this procedure, the optimizer will alternate between the two screens until the specified convergence threshold is reached. Note, that using two consequent locations effectively removes the dependency from $\beta_{x,y}$ as betatron functions could only have

¹ This work is supported by the DOE contract No.DEAC02-07CH11359 to the Fermi Research Alliance LLC. The work of A.H. is supported by the US Department of Energy under contract No. DE-SC0011831 with Northern Illinois University.

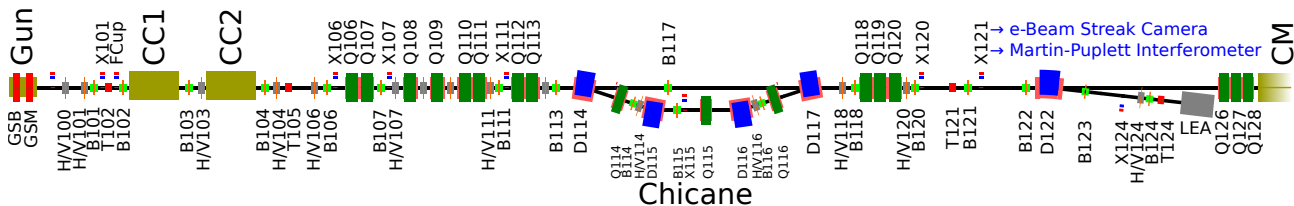


Figure 1: IOTA/FAST beamline. Photoelectrons are born and initially are accelerated in a normal conducting L-band RF gun, then further boosted up to 52 MeV in two L-band SRF booster cavities (CC1,CC2). The electron beam is then matched in the quadrupole channel into the ILC-type cryomodule (CM) that gives the beam its final energy of 301 MeV. For IOTA operations the cryomodule is operated at a lower gradient to obtain 150 MeV electrons. Both low and high energy beamlines have experimental areas located near low- and high-energy adsorbers. For a detailed description of the beamline see Ref. [2].

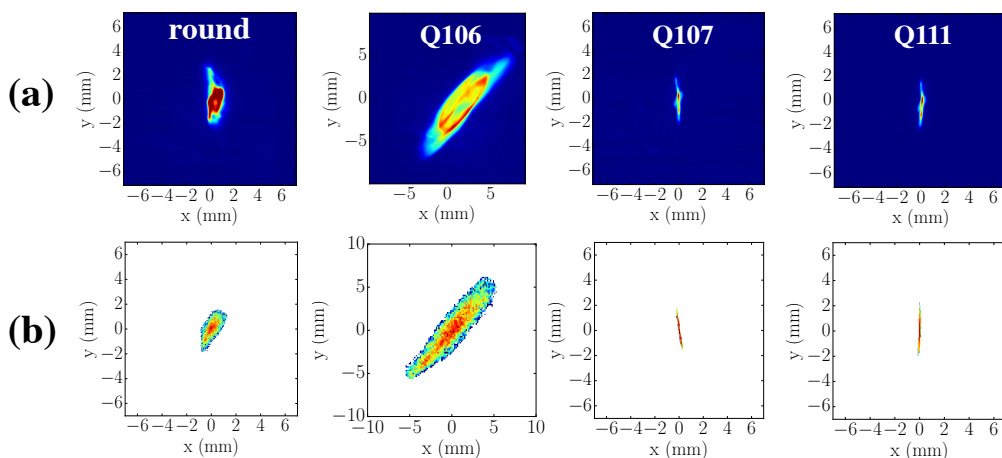


Figure 2: Demonstration of the CAM removal process in the experiment (a) and simulations (b) for the case of a vertical flat beam. The transverse beam density was recorded at X111 location.

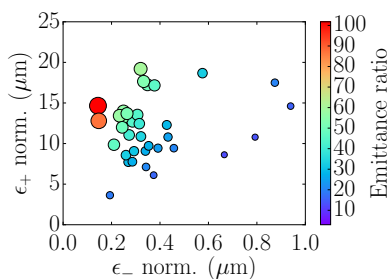


Figure 3: Demonstration of beam-based optimization of the eigenemittance mapping for the case of vertical/horizontal flat beam. The size (color) of the disks increases with the measured beam flatness ratio. Red disks correspond to the best emittance ratios obtained for horizontal/vertical flat beams.

one local minima in the free space, thus optimizing $\epsilon_{x,y}$. The method was found to be efficient and fast in flat beam emittances optimization. However, the beam optics constraints and the screen resolution are the main limitations of this technique. In order to further optimize the resulting flat beam

emittances, a direct single-shot emittance measurement is required, e.g. with an intercepting mask. The performance of the beam-based flat beam optimizer is demonstrated in Fig. 3.

FLAT BEAM COMPRESSION

A numerical model for FAST beamline with a chicane parameters presented in Fig. 1 was implemented in the IMPACT-R code [14]. The simulations included space-charge forces and one-dimensional CSR effects when particles were propagated through the chicane. In order to introduce the energy spread required for bunch compression, the second booster cavity was run off-crest. The maximum compression in the FAST beamline corresponds to the second booster cavity phase to be -30 degrees off-crest, and maximum decompression is achieved when it is +30 degrees off-crest. Numerical model also included the experimental RTFB adapter settings. The resulting lower emittance ϵ_- as a function of second booster cavity phase is plotted in Fig. 4. Additionally, Fig. 4 provides bunch duration measurement as a function of booster cavity phase performed with the streak camera; see Fig. 1. As expected, when ϵ_- is mapped onto horizontal plane, the emittance is significantly degraded after the

Content from this work may be used under the terms of the CC BY 3.0 licence (© 2018). Any distribution of this work must maintain attribution to the author(s), title of the work, publisher, and DOI.

maximum compression (a 6-fold increase is observed). In contrast, when ϵ_- is mapped onto the vertical plane, the emittance dilution at the maximum-compression phase reduced to 1.75 times its initial value owing to the large value of ϵ_+ in the horizontal plane. It has been shown via numerical simulations that the emittance growth in the latter case can be further mitigated by adjusting the beam focusing in the chicane [3]. The experimentally measured compressed ver-

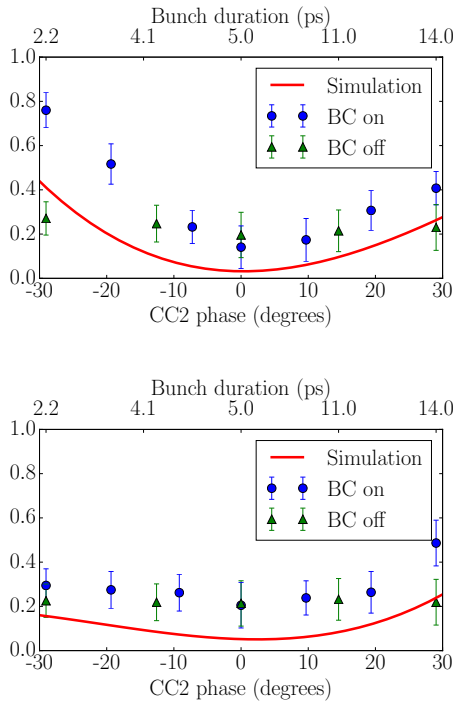


Figure 4: Compressed (BC on) and non-compressed (BC off) vertical (top) and horizontal (bottom) flat beam smaller emittances measured as a function of the second capture cavity phase compared with IMPACT-T simulations.

tical and horizontal emittances are presented in Fig. 4. The emittance growth is in an excellent agreement with the previous experimental conclusions and numerical simulations for both cases of round and flat beam [3,4]. In the case of a maximally compressed vertical flat beam, the lower emittance growth is about a factor of 4. For the maximally compressed horizontal flat beam, the emittance dilution is only a factor of 1.5, which is consistent with IMPACT-T simulations. Figure 4 shows the resulting comparison between measured experimental values and simulations. The dilution of the upper emittance ϵ_+ in both horizontal and vertical flat beam cases measured to be much less significant (about 15% in case of maximum compression), which is within the estimated error bar for all the measurements. In Fig. 5, total ϵ_{4D} growth for flat beam compression is compared to the case of a round beam of the same charge and size at the photocathode. The case of vertical flat-beam ($\epsilon_y \gg \epsilon_x$) does not present a significant improvement in ϵ_{4D} preservation, while horizontal flat beams mitigate the ϵ_{4D} dilution by a factor ~ 2 . The nu-

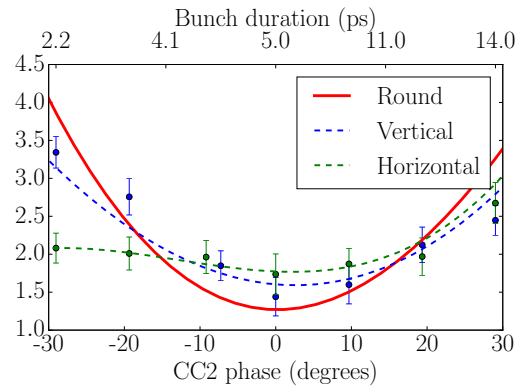


Figure 5: Measured ϵ_{4D} as a function of second booster cavity phase for both vertical and horizontal flat beams. Solid line corresponds to the simulated case of a round non-magnetized beam of the same RMS size at the photocathode. Dashed lines are drawn for reference.

merical simulations indicate a dependency of the flat beam emittances from the phases of the booster cavities. Due to RF-uncertainty of about 1 MV/m in both capture cavities, the degree of freedom associated with the minimizing of the energy spread was not available for a fine beam-based optimization. This limitation impacts the measured value of the RMS beam size σ_{mes} as [15]:

$$\sigma_{mes} = \sqrt{\sigma_0^2 + \sigma_{res}^2 + (\eta\delta)^2},$$

where σ_0 is the real RMS beam size, η is the RTFB adapter dispersion and δ is the energy spread. The error in measured σ_{mes} , in turn, propagates to the resulting emittance value.

CONCLUSIONS

For the first time we demonstrated an experimental setup with a CAM beam transformed into a compressed horizontal flat beam. This type of a beam was found to better preserve the total ϵ_{4D} . At FAST, such a setup can lead to a better quality beam to be delivered to the high-energy beamline and IOTA ring. Additionally, a reverse flat-to-round transformation can be performed after propagating through the bunch compressor. This technique can serve as a method of transporting CAM beams in the accelerator [16].

ACKNOWLEDGEMENTS

Authors are grateful to the FAST team members and Fermilab's AD and TD support departments. We especially want to thank A. Lumpkin and R. M. Thurman-Keup for their help with the streak camera measurement, S. Nagaitsev and A. Valishev for the in-depth discussions.

REFERENCES

- [1] Ya. Derbenev. Adapting optics for high-energy electron cooling, UM-HE-98-04-A, (1998).

- [2] S. Antipov, *et al*, *Journal of Instrumentation*, 12(03):T03002, (2017).
- [3] J. Zhu, P. Piot, D. Mihalcea, and C. R. Prokop. *Phys. Rev. ST Accel. Beams*, **17**, 084401 (2014).
- [4] Bane, K. L. F, *et al*, *Phys. Rev. ST Accel. Beams*, **12**, 030704 (2009).
- [5] Y. S. Derbenev, J. Rossbach, E. L. Saldin, and V. D. Shiltsev. DESY TESLA-FEL 95-05 (1995).
- [6] C. Mitchell, J. Qiang, P. Emma, *Phys. Rev. ST Accel. Beams*, **16**, 060703 (2013).
- [7] A. Halavanau, *et al*, *Proc. of IPAC2018*, Vancouver, Canada, paper THPAK061, (2018).
- [8] A. Halavanau, `MAGNETOPTIMIZER`
<https://github.com/NIUaard/MagnetOptimizer>, (2017).
- [9] M. Borland. *Advanced Photon Source*, LS-287, (2000).
- [10] R. Brinkmann, Ya. Derbenev, and K. Flottmann. *Phys. Rev. ST Accel. Beams*, **4**, 053501 (2001).
- [11] S. Nagaitsev and A. Shemyakin, FERMILAB-TM-2107, (2000).
- [12] K. J. Kim. *Phys. Rev. ST Accel. Beams*, 6:104002, (2003).
- [13] P. Piot and A. Halavanau, *FERMILAB-CONF-16-464-AD-APC*, (2016).
- [14] J. Qiang *IMPACT-T reference manual*, LBNL-62326, (2007).
- [15] Y. Sun, "Angular-momentum-dominated electron beams and flat-beam generation", Ph.D. Dissertation, University of Chicago, Chicago, USA (2005).
- [16] P. Piot and Y. E. Sun, *FERMILAB-CONF-14-142-APC* (2014).